Splitting of conductance resonance through a magnetic quantum dot in graphene

Nojoon Myoung,[1] Jung-Wan Ryu,[2] Hee Chul Park,[2] Seung Joo Lee,[3] and Sungjong Woo[2,*]
[1]*Department of Physics Education, Chosun University, Gwangju 61452, Republic of Korea*
[2]*Center for Theoretical Physics of Complex Systems, Institute for Basic Science (IBS), Daejeon 34126, Republic of Korea*
[3]*Quantum-functional Semiconductor Research Center, Dongguk University, Seoul 04620, Republic of Korea*

(Received 31 October 2018; revised manuscript received 1 July 2019; published 31 July 2019)

We report a dual resonance feature in the ballistic conductance through a quantum Hall graphene nanoribbon with a magnetic quantum dot. Such a magnetic quantum dot localizes Dirac fermions exhibiting anisotropic eigenenergy spectra with broken time-reversal symmetry. Interplay between the localized states and quantum Hall edge states is found to be twofold, showing Breit-Wigner and Fano resonances, which is reminiscent of a double quantum dot system. By fitting the numerical results with the Fano-Breit-Wigner line shape from the double quantum dot model, we demonstrate that the twofold resonance is due to the valley mixing that comes from the coupling of the magnetic quantum dot with quantum Hall edge channels; an effective double quantum dot system emerges from a single magnetic quantum dot in virtue of the valley degree of freedom. It is further confirmed that the coupling is weaker for the Fano resonance and stronger for the Breit-Wigner resonance.

DOI: 10.1103/PhysRevB.100.045427

I. INTRODUCTION

A quantum dot (QD), one of the most important ingredients in nanotechnology, shows many unique properties in the mesoscopic regime between bulk semiconductors and individual atoms such as Coulomb blockade [1,2] and Kondo effect [3,4]. Among such applications is included the electronic transport through quantum dots, which provides promising routes toward cutting-edge technology such as quantum computing [5–10] and resonant tunneling devices [1,11,12]. For the coherent transport in quantum dot devices, however, an extremely clean and low temperature environment is generally required.

On the other hand, graphene, a two-dimensional carbon crystal with two distinct Dirac cones having linear dispersion in the electronic band structure, shows prominent transport behavior with high carrier mobility and long mean free path making graphene promising as a candidate material to succeed silicon in the nanoelectronic industry [13,14]. Graphene's superiority can be further enhanced utilizing specific substrates, especially hexagonal boron nitride together with an encapsulation technique [13], so that experimental investigations on theoretical predictions that require ballistic coherent transport over a micrometer scale is made possible such as Veselago lens [15–17], valley-isospin dependent quantum Hall effects [18], etc.

While substantial effort has been made to investigate transport through electrostatic QDs in graphene [19–23], electrostatically controllable quantum dots using local gates, which are common in two-dimensional electron gas systems, is difficult to be applied due to the Klein tunneling. Under magnetic field, on the other hand, it is possible to confine the motion of electrons at the interface of the field strength [24–27]. Such localized electronic states can be understood as snake trajectories which is reminiscent of quantum Hall interface states at a *p-n* junction [28–35]. At a boundary of a circular field-free domain within a homogeneous magnetic field, the snake trajectory of an electron results in a closed orbit confining the electronic states within the field-free region, generating a magnetic quantum dot (MQD). Such localized states with discrete energy spectra have been known to exist within a MQD that can be realized by screening a homogeneous magnetic field locally [36]. With MQDs, one can bypass the Klein tunneling problem [37–40].

In the present work we investigate electronic transport in graphene nanoribbons where a MQD is located between two quantum Hall edge channels (Fig. 1). We analyze the feature of resonance tunnelings in the conductance through the MQD, evidencing the existence of the localized states in the MQD. The results of the analysis are discussed in the context of the coupling between the extended edge states and the discrete localized states in the MQD, showing the Breit-Wigner and Fano resonances at specific energies corresponding to the energy levels of the MQD.

The present paper is composed of the following sections. Section II outlines the MQD in a 2D graphene sheet. We offer a preliminary study of eigenenergy spectra for the MQD which indicate the formation of localized states. The continuity of the wave functions are assumed across the boundary of the MQD in the analytical calculations. In Sec. III, numerical results of the ballistic conductance across the MQD in a graphene nanoribbon are analyzed. We compute transport properties numerically with the scattering matrix formalism based on the tight-binding method. Resulting resonant features in the conductance spectra are discussed addressing Fano and Breit-Wigner resonances. We additionally remark on the dot–edge-distance dependence of the splitting between

*sjwoo@ibs.re.kr

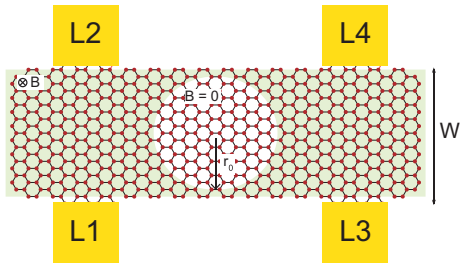

FIG. 1. Schematic diagram of the system considered in this work. The external magnetic field is expelled out in the circular area characterized by radius r_0. There are four leads labeled as L1, L2, L3, and L4 for scattering matrix calculations from a lead to another lead.

two types of resonances. Finally, Sec. IV brings our work to a conclusion.

II. ELECTRONIC PROPERTIES OF MQD

We now discuss localized-state solutions in our system which is modeled as a circularly symmetric quantum dot using magnetic fields. A MQD with a radius r_0 is modeled as $\vec{B} = B\hat{z}$ for $r > r_0$ and $\vec{B} = 0$ for $r < r_0$. Such a nonuniform magnetic field can be practically realized by top-gated structures using a disklike superconductor electrode with a thin dielectric spacer such as few-layered h-BN between the top local gate and graphene. Although we have noted that the eigenstate solutions of the same system is given by De Martino *et al.* [37], full spectra necessary for the analysis of our transport calculations are not provided in detail. On that account, we include a brief description of the solution with further analysis of the spectra with density profiles of wave functions in this paper.

A Dirac Hamiltonian of the system reads

$$H_v = v_F(\pi_x\sigma_x + v\pi_y\sigma_y) + U\sigma_0, \tag{1}$$

where $v_F \simeq 10^6$ ms^{-1} is the Fermi velocity, $\pi_i = p_i + eA_i$ is the kinetic momentum under magnetic field, σ_x and σ_y are Pauli matrices, σ_0 is the unity matrix, and $v = \pm 1$ for K and K' valleys. For simplicity, we suppose that the system is electrostatically homogeneous; $U = 0$. By choosing an appropriate gauge in a plane polar coordinate, the Dirac equations are written as

$$\hbar v_F e^{-i\phi}\left[-i\frac{\partial}{\partial r} - iv\left(-\frac{i}{r}\frac{\partial}{\partial\phi} + \frac{eA_\phi}{\hbar}\right)\right]\psi_{B,v} = E\psi_{A,v}, \tag{2}$$

$$\hbar v_F e^{i\phi}\left[-i\frac{\partial}{\partial r} + iv\left(-\frac{i}{r}\frac{\partial}{\partial\phi} + \frac{eA_\phi}{\hbar}\right)\right]\psi_{A,v} = E\psi_{B,v}, \tag{3}$$

where $A_\phi = \frac{B}{2r}(r^2 - r_0^2)$ is nonzero only for $r > r_0$. Due to the rotational symmetry, the solution of the Dirac equation has the form $\Psi(r,\phi) = e^{im\phi}R(r)$, where m is an integer and $R(r) = (R_A, e^{i\phi}R_B, e^{i\phi}R_{A'}, R_{B'})^T$ [41,42]. In the following, all the formulas are dimensionless based on magnetic length and Landau energy gap: $l_B = \sqrt{\hbar/eB}$ for the length and $E_0 = \sqrt{2}\hbar v_F/l_B = \sqrt{2\hbar v_F^2 eB}$ for the energy. For K valley, eliminating ψ_B in Eqs. (2) and (3) yields

$$\left(\frac{d^2}{dr^2} + \frac{1}{r}\frac{d}{dr} - \frac{m^2}{r^2} + 2E^2\right)R_A = 0, \tag{4}$$

for $r < r_0$ and

$$\left(\frac{d^2}{dr^2} + \frac{1}{r}\frac{d}{dr} - \frac{m_{eff}^2}{r^2} - \frac{1}{4}r^2 - 2m_{\rm eff} - 2 + 2E^2\right)R_A = 0, \tag{5}$$

for $r > r_0$, where $m_{\rm eff} \equiv m - s$. Here $s \equiv B\pi r_0^2 e/h$ is the "missing" flux, which indicates the amount of magnetic flux screened out from the MQD. The solutions for the differential equations are Bessel's function of the first kind for $r < r_0$ and a confluent hypergeometric function for $r > r_0$ and ψ_B can accordingly be obtained using Eq. (3) [37].

On the other hand, for K' valley, exactly the same differential equations, Eqs. (4) and (5), are obtained for $\psi_{B'}$ by eliminating $\psi_{A'}$ from Eqs. (2) and (3) with $v = -1$. This guarantees degeneracies in the spectrum between the two valleys. The valley degeneracy can only be lifted, but not sufficiently, by breaking A-B sublattice symmetry such as infinite mass boundary condition [41,43–45], which is not the case for a magnetic gauge potential like our system. In fact, the splitting of the resonance peaks in the conductance spectrum, the main topic of this paper, is due to the valley mixing, which would not occur if the degeneracy is lifted.

The eigenenergies labeled by an additional quantum number n can be obtained by imposing the continuity condition of $R(r)$ at $r = r_0$ for each value of m [37] (Fig. 2). As is mentioned above, the two valleys are degenerate in the eigenenergy spectra. Due to the broken time-reversal symmetry, the eigenenergies exhibit asymmetric behavior with respect to the sign of m. For small $|m|$ there are small discrepancies between time-reversal partners E_{nm} and $E_{n,-m}$. It is due to the fact that the wave functions with small $|m|$ mainly reside within the quantum dot where the magnetic field is zero so that the time-reversal symmetry is barely broken. On the other hand, for larger $|m|$, larger discrepancies are observed between time-reversal partners.

One noticeable analysis is the direction of the persistent current along the MQD boundary, defined by $I_{nm} = (1/\hbar)\partial E_{nm}/\partial m$. The signs of I_{nm} indicates that the semiclassical trajectories for the localized states can be either clockwise or counterclockwise rotation of snake orbits along the MQD boundary [36]. Interestingly, there is a flat eigenenergy spectrum at zero energy, not depending on m. The zero-energy states are understood by solving the differential equation with $E = 0$. The resulting eigenstates of the zero energy are given by a linear summation of electron states on $A(B)$ sites and hole states on $B(A)$ sites [42].

Analysis of each energy eigenstate Ψ_{nm} corresponding to E_{nm} shows that n and m are the radial and angular quantum numbers, respectively. Each eigenstate Ψ_{nm} describes how the localized states are formed in the MQD. Some of the localized state wave functions are plotted in Figs. 2(b)–2(g). Note that the intensities of the wave functions are isotropic but dependent on quantum numbers n and m. The wave functions for $m = 0$ (Ψ_{10} and Ψ_{20}) exhibit their maxima at the center

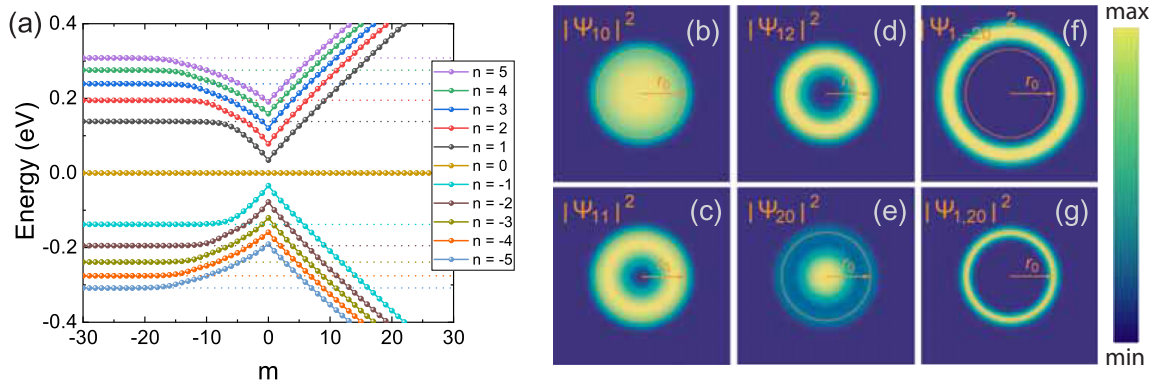

FIG. 2. (a) Eigenenergy spectra ε_{nm} of the magnetic quantum dot. Dotted lines indicate Landau levels of graphene under a homogeneous magnetic field. Colored solid dots correspond to ε_{nm} values, connected by the same-color solid lines of which colors refer to different n indices. (b)–(g) Localized state intensities of the MQD for different indices. Dotted lines indicate the boundary of the MQD.

of the MQD, whereas the wave functions for $m \neq 0$ (Ψ_{11} and Ψ_{12}) show their minima at the MQD center. Especially, as displayed in Fig. 2(f), the localized state wave functions for $m = -20$ are found totally outside the MQD boundary, forming cyclotron orbits in a uniform-magnetic-field region. As we already mentioned, this is consistent with the finding that E_{nm} converges to nth Landau level as $|m|$ increases with $m < 0$. The slope of the linear dispersion can be estimated to be the kinetic energy of a Dirac particle located near the boundary of the QD, $E \sim m/(\sqrt{2}r_0)$. The critical value for m where the dispersion changes from linear to flat Landau levels can be estimated by equating the linear dispersion with the corresponding Landau level energy which is identity in our magnetic unit for $n = 1$ so that $m_c \sim \sqrt{2}r_0 \approx 10$. This value matches reasonably well with the dispersions in Fig. 2(a). On the other hand, in Fig. 2(g), $\Psi_{1,20}$ exhibits a distinct feature to $\Psi_{1,-20}$ because of the broken time-reversal symmetry. The localized state wave function for $m = 20$ mainly reside within the MQD.

III. BALLISTIC CONDUCTANCE THROUGH MAGNETIC QUANTUM DOT

So far we have studied the eigenenergies and localized state wave function of the isolated MQD in an infinitely large graphene sheet. In practice, as depicted in Fig. 1, the sizes of graphene samples for conductance measurements are finite, and quantum Hall edge channels are formed along the edge of the sample. For a MQD on such a finite-sized sample, the localized states are inevitable to have coupling with the extended edge states of the sample, leaving resonances in the conductance spectrum. In this study we use a 98.4-nm-wide graphene nanoribbon with armchair edges to take into account the valley-isospin-dependent quantum Hall effects [18]. A magnetic quantum dot is introduced at the center of the nanoribbon with a radius of 44.3 nm which is about 5 nm apart from both edges. In our simulations, we have used $B = 15.7$ T for which the cyclotron radius $r_c = 6.5$ nm, so that the aforementioned coupling is substantial. As a consequence of the coupling, Dirac fermions coming from one edge can be transferred to the other edge through the MQD. The conductance from L1 to L2 in Fig. 1 is numerically calculated using S-matrix formalism based on tight-binding approach with KWANT package [46,47], in order to check how Dirac fermions pass through the MQD between the two edges. Hopping energy of 3 eV is used between nearest neighbor p_z orbitals.

Figure 3 presents the conductance as a function of the energy of Dirac fermions. One can see that there are a number of resonance peaks. Without MQD the conductance should be zero since two quantum Hall edge channels cannot talk to each other in the ballistic regime. Figures 3(a) and 3(b) show that energies of the resonance peaks match well to the eigenenergies of the localized states in the MQD. Such correspondence implies that the conductance resonances are indeed consequences of the coupling between the edge channels and the localized states on the MQD. Figures 3(c)–3(f) demonstrate that each resonance does result from the localized states in the MQD with a good agreement with the analytic solutions given in Figs. 2(b)–2(e).

A detailed look into Fig. 3 further shows interesting features within the resonance peaks. There are two distinct shapes of resonances for each localized states, broad and symmetric peaks for the Breit-Wigner resonances, and sharp and asymmetric peaks for the Fano resonances. A Breit-Wigner resonance occurs when an extended state is strongly coupled with localized states. On the other hand, a Fano resonance is an interference effect due to the weak coupling between extended and localized states. Such conductance spectra are discovered in charge transport through coupled double quantum dots, where Breit-Wigner and Fano resonances occur at energies corresponding to bonding and antibonding of the two dots [48]. In this study, even though there is only one MQD, there are two degenerate valley states, which are split with valley mixing due to the coupling with the edge channels [18,49–51]. Quantitative analysis of the coexistence of Fano and Breit-Wigner resonances is done by performing numerical fitting using the double QD model [48], finding the peak positions E_{Fano} and E_{BW}, and their widths γ_{Fano} and γ_{BW}.

We first note that the Fano peak in a peak splitting on a MQD has lower energy compared to the Breit-Wigner peak, which is contrary to a general double QD. In a double QD, the Fano peak is for the antibonding state of two dots which has higher energy than the bonding. A graphene nanoribbon with

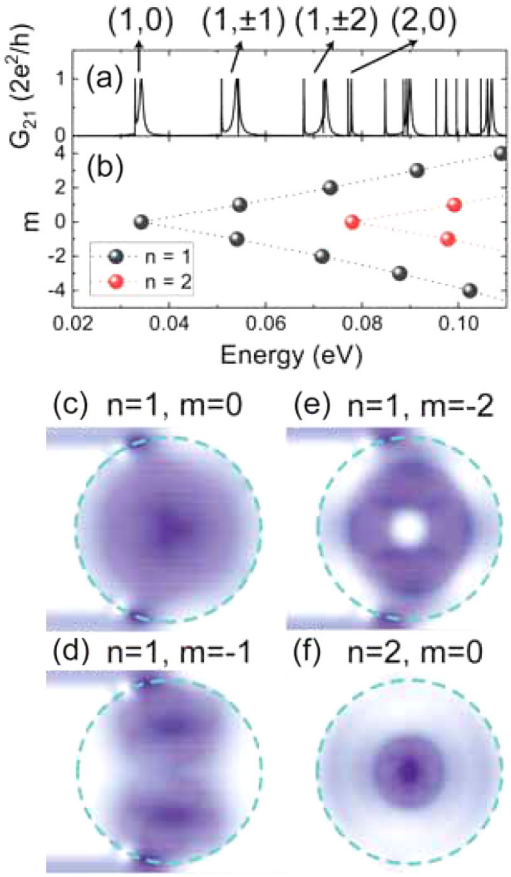

FIG. 3. (a) Conductance calculated between L1 and L2 leads as a function of Dirac fermion energy. First four resonances are denoted by their corresponding localized states labeled as (n, m). (b) Enlargement of the eigenenergy spectra focusing on the lower eigenenergies. Black and red symbols represent the eigenenergy bands for $n = 1$ and $n = 2$, respectively. Parameter $r_0 = 4.2$ is used in the eigenenergy calculation. (c)–(f) Image plots of wave functions of the scattering region in S-matrix formalism acquired from KWANT codes, for given Dirac fermion energies corresponding to the first four resonances in the conductance spectra (a). The dashed line indicates the size of the MQD. Note that the image plots are normalized by their maximum values for clarity of viewing.

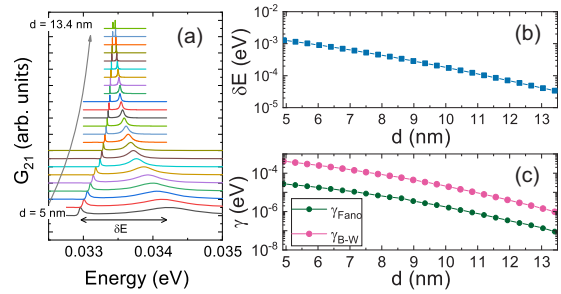

FIG. 4. (a) Conductance spectra around the first resonance peaks as functions of Dirac fermion energy for various edge-dot distances from $d = 5$ to 13.4 nm with an increment 0.37 nm. (b) The energy splitting δE as a function of d from the fitted data. (c) Coupling strengths of Fano and Breit-Wigner resonances, γ_{Fano} and γ_{BW}, from the numerical fitting as functions of d.

armchair edges allows only antisymmetric states of valleys, $\psi_K - \psi_{K'}$ [52,53]. With a MQD, although symmetric states of two valleys are allowed due to the partial existence of zigzag edge along the boundary of the dot, antisymmetric states are still preferred energetically, i.e., have lower energy. Symmetric valley mixing has the disbenefit of kinetic energy at the armchair edge while antibonding of two dots in the double QD model has the disbenefit of kinetic energy at the node of wave function between the two dots.

In order to further understand the valley splitting in the MQD with the edge channels, we investigate how the conductance spectra for the resonances behave depending on the distance between the MQD and the edges d. Figure 4(a) shows the d dependence of the conductance resonances in case of $(n, m) = (1, 0)$. It is clearly seen that the Fano and Breit-Wigner resonant peaks become closer to each other as d increases, eventually converging to a single peak for sufficiently large d. It is because the MQD gets decoupled from the edge. The exponential behaviors of the resonant peak splitting $\delta E = E_{\text{BW}} - E_{\text{Fano}}$, and coupling strengths γ_{Fano} and γ_{BW}, in terms of d [Figs. 4(b) and 4(c)] imply that such valley splitting stems from the coupling with the edge; the coupling strength between the MQD and the edge is proportional to wave function overlap between the localized states and the edge channels. Figure 4(c) also confirms the fact that the coupling for the Fano resonance should be much weaker than that for the Breit-Wigner resonances. The two-level splitting for a single MQD is a unique feature of a graphene nanoribbon with the presence of valley isospin degeneracy.

IV. CONCLUSIONS

In conclusion, using both numerical and analytical approaches, we have shown that the quantum Hall conductance on a graphene sample with a MQD exhibits two distinguished resonant spectra, Fano and Breit-Wigner resonances, as a consequence of the valley mixing in the MQD. Even though an isolated MQD has valley degeneracy, the coupling between the MQD and edge channels leads to valley mixing for a finite-size quantum Hall graphene system. By fitting the resonant spectra, we have demonstrated that the two-level splitting due to the valley mixing becomes smaller as the distance between the MQD and edge channels increases, accompanied with narrower spectral widths of resonances. It shows that the valley mixing is due to the wave function overlap between the MQD and the edge channel. Analysis of the numerical results has confirmed that the coupling for the Fano resonances is much weaker than that for the Breit-Wigner resonances. When compared to conventional two-dimensional electron gas systems, the coexistence of Fano and Breit-Wigner resonances for a single dot structure on a graphene nanoribbon is a unique phenomena, which is due to the valley degree of freedom. The reason why the Fano peak in a MQD has lower energy than the Breit-Wigner peak differently from a double QD model is also explained from the perspective of edge coupling. The last comment we want to add is that a sub-Kelvin temperature, required for an experimental measurement of the sharp Fano resonances, is experimentally accessible with the most current technologies [54].

ACKNOWLEDGMENTS

This work is supported by National Research Foundation of Korea (Grants No. NRF-2017R1C1B5076824, No. IBS-R024-D1, and No. NRF-2016R1D1A1B04-935798), Korea Institute for Advanced Study (KIAS), and Chosun University (2017). The author thank H. Choi for fruitful discussion about the experimental feasibility of our findings.

[1] C. W. J. Beenakker, Phys. Rev. B **44**, 1646 (1991).
[2] E. Leobandung, L. Guo, Y. Wang, and S. Y. Chou, Appl. Phys. Lett. **67**, 938 (1995).
[3] S. M. Cronenwett, T. H. Oosterkamp, and L. P. Kouwenhoven, Science **281**, 540 (1998).
[4] S. Sasaki, S. De Franceschi, J. M. Elzerman, W. G. van der Wiel, M. Eto, S. Tarucha, and L. P. Kouwenhoven, Nature (London) **405**, 764 (2000).
[5] D. Loss and D. P. DiVincenzo, Phys. Rev. A **57**, 120 (1998).
[6] A. Steane, Rep. Prog. Phys. **61**, 117 (1998).
[7] T. D. Ladd, F. Jelezko, R. Laflamme, Y. Nakamura, C. Monroe, and J. L. O'Brien, Nature (London) **464**, 45 (2010).
[8] D. Aasen, M. Hell, R. V. Mishmash, A. Higginbotham, J. Danon, M. Leijnse, T. S. Jespersen, J. A. Folk, C. M. Marcus, K. Flensberg, and J. Alicea, Phys. Rev. X **6**, 031016 (2016).
[9] C. Godfrin, S. Thiele, A. Ferhat, S. Klyatskaya, M. Ruben, W. Wernsdorfer, and F. Balestro, ACS Nano **11**, 3984 (2017).
[10] T. F. Watson, S. G. J. Philips, E. Kawakami, D. R. Ward, P. Scarlino, M. Veldhorst, D. E. Savage, M. G. Lagally, M. Friesen, S. N. Coppersmith, M. A. Eriksson, and L. M. K. Vandersypen, Nature (London) **555**, 633 (2018).
[11] F. Simmel, R. H. Blick, J. P. Kotthaus, W. Wegscheider, and M. Bichler, Phys. Rev. Lett. **83**, 804 (1999).
[12] J. Velsaco Jr., J. Lee, D. Wong, S. Kahn, H.-Z. Tsai, J. Costello, T. Umeda, T. Taniguchi, K. Watanabe, A. Zettl, F. Wang, and M. F. Crommie, Nano Lett. **18**, 5104 (2018).
[13] P. J. Zomer, S. P. Dash, N. Tombros, and B. J. van Wees, Appl. Phys. Lett. **99**, 232104 (2012).
[14] A. K. Geim and K. S. Novoselov, Nat. Mater. **6**, 183 (2007).
[15] V. V. Cheianov, V. Fal'ko, and B. L. Altshuler, Science **315**, 1252 (2007).
[16] G.-H. Lee, G.-H. Park, and H.-J. Lee, Nat. Phys. **11**, 925 (2015).
[17] S. Chen, Z. Han, M. M. Elahi, K. M. Masum Habib, L. Wang, B. Wen, T. Gau, Y. Taniguchi, K. Watanabe, J. Hone, A. W. Ghosh, and C. R. Dean, Science **353**, 1522 (2016).
[18] J. Tworzydlo, I. Snyman, A. R. Akhmerov, and C. W. J. Beenakker, Phys. Rev. B **76**, 035411 (2007).
[19] J. H. Bardarson, M. Titov, and P. W. Brouwer, Phys. Rev. Lett. **102**, 226803 (2009).
[20] J. Lee, D. Wong, J. Velasco, Jr., J. F. Rodriguez-Nieva, S. Kahn, H.-Z. Tsai, T. Taniguchi, K. Watanabe, A. Zettl, F. Wang, L. S. Levitov, and M. F. Crommie, Nat. Phys. **12**, 1032 (2016).
[21] N. M. Freitag, L. A. Chizhova, P. Nemes-Incze, C. R. Woods, R. V. Gorbachev, Y. Cao, A. K. Geim, K. S. Novoselov, J. Burgdörfer, F. Libisch, and M. Morgenstern, Nano Lett. **16**, 5798 (2017).
[22] S. Wang, N. Kharche, E. C. Girão, X. Feng, K. Müllen, V. Meunier, R. Fasel, and P. Ruffieux, Nano Lett. **17**, 4277 (2017).
[23] M. Mirzakhani, M. Zarenia, P. Vasilopoulos, and F. M. Peeters, Phys. Rev. B **95**, 155434 (2017).
[24] T. K. Ghosh, A. De Martino, W. Häusler, L. Dell'Anna, and R. Egger, Phys. Rev. B **77**, 081404(R) (2008).
[25] L. Oroszlány, P. Rakyta, A. Kormányos, C. J. Lambert, and J. Cserti, Phys. Rev. B **77**, 081403(R) (2008).
[26] S. Park and H.-S. Sim, Phys. Rev. B **77**, 075433 (2008).
[27] T. Taychatanapat, J. Y. Tan, Y. Yeo, K. Watanabe, T. Taniguchi, and B. Özylmaz, Nat. Commun. **6**, 6093 (2015).
[28] J. R. Williams, L. DiCarlo, and C. M. Marcus, Science **317**, 638 (2007).
[29] D. A. Abanin and L. S. Levitov, Science **317**, 641 (2007).
[30] F. Amet, J. R. Williams, K. Watanabe, T. Taniguchi, and D. Goldhaber-Gordon, Phys. Rev. Lett. **112**, 196601 (2014).
[31] N. N. Klimov, S. T. Le, J. Yan, P. Agnihotri, E. Comfort, J. U. Lee, D. B. Newell, and C. A. Richter, Phys. Rev. B **92**, 241301(R) (2015).
[32] S. Morikawa, S. Masubuchi, R. Moriya, K. Watanabe, T. Taniguchi, and T. Machida, Appl. Phys. Lett. **106**, 183101 (2015).
[33] D. S. Wei, T. van der Sar, J. D. Sanchez-Yamagishi, K. Watanabe, T. Taniguchi, P. Jarillo-Herrero, B. I. Halperin, and A. Yacoby, Sci. Adv. **3**, e1700600 (2017).
[34] N. Myoung and H. C. Park, Phys. Rev. B **96**, 235435 (2017).
[35] P. Makk, C. Handschin, E. Tóvári, K. Watanabe, T. Taniguchi, K. Richter, M.-H. Liu, and C. Schönenberger, Phys. Rev. B **98**, 035413 (2018).
[36] H.-S. Sim, K.-H. Ahn, K. J. Chang, G. Ihm, N. Kim, and S. J. Lee, Phys. Rev. Lett. **80**, 1501 (1998).
[37] A. De Martino, L. Dell'Anna, and R. Egger, Phys. Rev. Lett. **98**, 066802 (2007).
[38] B. Trauzettel, D. V. Bulaev, D. Loss, and G. Burkard, Nat. Phys. **3**, 192 (2007).
[39] N. Myoung and G. Ihm, Physica. E **42**, 70 (2009).
[40] M. Esmailpour, Physica B **534**, 150 (2018).
[41] P. Recher, J. Nilsson, G. Burkard, and B. Trauzettel, Phys. Rev. B **79**, 085407 (2009).
[42] M. Grujić, M. Zarenia, A. Chaves, M. Tadić, G. A. Farias, and F. M. Peeters, Phys. Rev. B **84**, 205441 (2011).
[43] J. G. Pedersen and T. G. Pedersen, Phys. Rev. B **85**, 035413 (2012).
[44] P. Rakyta, E. Tóvári, M. Csontos, S. Csonka, A. Csordás, and J. Cserti, Phys. Rev. B **90**, 125428 (2014).
[45] P. Rakyta, M. Vigh, A. Csordás, and J. Cserti, Phys. Rev. B **91**, 125412 (2015).
[46] P. R. Amestoy, I. S. Duff, J. S. Koster, and J. Y. L'Excellent, SIAM J. Matrix Anal. Appl. **23**, 15 (2001).
[47] C. W. Groth, M. Wimmer, A. R. Akhmerov, and X. Waintal, New J. Phys. **16**, 063065 (2014).
[48] M. L. Ladrón de Guevara, F. Claro, and P. A. Orellana, Phys. Rev. B **67**, 195335 (2003).
[49] A. R. Akhmerov and C. W. J. Beenakker, Phys. Rev. Lett. **98**, 157003 (2007).

[50] T. Sekera, C. Bruder, E. J. Mele, and R. P. Tiwari, Phys. Rev. B **95**, 205431 (2017).
[51] C. Handschin, P. Makk, P. Rickhaus, R. Maurand, K. Watanabe, T. Taniguchi, K. Richter, M.-H. Liu, and C. Schönenberger, Nano Lett. **17**, 5389 (2017).
[52] K.-i. Sasaki, K. Wakabayashi, and T. Enoki, J. Phys. Soc. Jpn. **80**, 044710 (2011).
[53] L. Brey and H. A. Fertig, Phys. Rev. B **73**, 195408 (2006).
[54] E. Weisz, H. K. Choi, M. Heiblum, Y. Gefen, V. Umansky, and D. Mahalu, Phys. Rev. Lett. **109**, 250401 (2012).